

Crystal Packing Mediates Enantioselective Ligand Recognition at the Peripheral Site of Acetylcholinesterase

Haim Haviv,^{†,‡} Dawn M. Wong,^{†,‡,§} Harry M. Greenblatt,[†] Paul R. Carlier,^{||}
Yuan-Ping Pang,[⊥] Israel Silman,[‡] and Joel L. Sussman^{*,†}

Contribution from the Departments of Structural Biology and Neurobiology, Weizmann Institute of Science, Rehovot 76100, Israel, Department of Chemistry, Virginia Tech, Blacksburg, Virginia 24061, and Computer-Aided Molecular Design Laboratory, Mayo Clinic College of Medicine, 200 First Street Southwest, Rochester, Minnesota 55905

Received March 20, 2005; E-mail: joel.sussman@weizmann.ac.il

Abstract: Recently, alkylene-linked heterodimers of tacrine (**1**) and 5-amino-5,6,7,8-tetrahydroquinolinone (**2**, hupryridone) were shown to exhibit higher acetylcholinesterase (AChE) inhibition than either monomeric **1** or **2**. Such inhibitors are potential drug candidates for ameliorating the cognitive decrements in early Alzheimer patients. In an attempt to understand the inhibition mechanism of one such dimer, (*RS*)-(±)-*N*-9-(1,2,3,4-tetrahydroacridinyl)-*N'*-5-[5,6,7,8-tetrahydro-2'(1'*H*)-quinolinonyl]-1,10-diaminododecane [(*RS*)-(±)-**3**] bisoxalate, the racemate was soaked in trigonal *Torpedo californica* AChE (*TcAChE*) crystals, and the X-ray structure of the resulting complex was solved to 2.30 Å resolution. Its structure revealed the **1** unit bound to the "anionic" subsite of the active site, near the bottom of the active-site gorge, as seen for the **1/TcAChE** complex. Interestingly, only the (*R*)-enantiomer of the **2** unit was seen in the peripheral "anionic" site (PAS) at the top of the gorge, and was hydrogen-bonded to the side chains of residues belonging to an adjacent, symmetry-related AChE molecule covering the gorge entrance. When the same racemate was soaked in orthorhombic crystals of *TcAChE*, in which the entrance to the gorge is more exposed, the crystal structure of the corresponding complex revealed no substantial enantiomeric selectivity. This observation suggests that the apparent enantiomeric selectivity of trigonal crystals of *TcAChE* for (*R*)-**3** is mainly due to crystal packing, resulting in preferential binding of one enantiomeric inhibitor both to its "host" enzyme and to its neighbor in the asymmetric unit, rather than to steric constraints imposed by the geometry of the active-site gorge.

Introduction

The principal role of the serine-hydrolase acetylcholinesterase (AChE; EC 3.1.1.7)¹ is termination of impulse transmission at cholinergic synapses by rapid hydrolysis of the neurotransmitter acetylcholine (ACh).² The crystal structure of *Torpedo californica*

nica AChE (*TcAChE*) revealed that its active site lies at the bottom of a deep and narrow gorge (20 Å), named the "active-site gorge" or "aromatic gorge", since nearly 70% of its surface is lined by the rings of 14 conserved aromatic amino acids.³ At the active site, the catalytic triad Ser200-His440-Glu327 is responsible for hydrolyzing the ester bond in ACh. At the "anionic" subsite of the active site (historically termed the "catalytic 'anionic' site", CAS), adjacent to the catalytic triad, the indole side chain of the conserved residue Trp84 makes a cation- π interaction with the quaternary amino group of ACh.⁴ A second aromatic residue, Phe330, is also involved in recognition of quaternary ligands and likely also of ACh.⁵ The conserved residue Trp279 is the major component of a second binding site, named the peripheral "anionic" site (PAS), ~14 Å from the active site, near the top of the gorge.⁵ A large body of kinetic studies, utilizing site-directed mutagenesis, supports these structural assignments.⁶

AChE inhibitors prolong the effects of the endogenously released neurotransmitter ACh in vivo. According to the

[†] Department of Structural Biology, Weizmann Institute of Science.
[‡] Department of Neurobiology, Weizmann Institute of Science.
[§] Present address: Department of Biochemistry, Hong Kong University of Science and Technology, Clear Water Bay, Kowloon, Hong Kong, China.
^{||} Virginia Tech.
[⊥] Mayo Clinic College of Medicine.
(1) Abbreviations: A β , β -amyloid; ACh, acetylcholine; AChE, acetylcholinesterase (EC 3.1.1.7); AD, Alzheimer's disease; AU, asymmetric unit; (*S,S*)-(-)-**4a**, (*S,S*)-(-)-bis-(10)-hupryridone dihydrochloride; (*S,S*)-(-)-**4b**, (*S,S*)-(-)-bis-(12)-hupryridone dihydrochloride; BChE, butyrylcholinesterase; BW, BW284C51; CAS, catalytic "anionic" site; ChE, cholinesterase; CCP4, Collaborative Computational Project, Number 4; CNS, Crystallography & NMR System; DECA, decamethonium; GAL, (-)-galanthamine; (-)-HupA, (-)-huperzine A; hupryridone or **2**, 5-amino-5,6,7,8-tetrahydroquinolinone; MES, 2-(*N*-morpholino)ethanesulfonic acid; NAG, *N*-acetyl-D-glucosamine; PAS, peripheral "anionic" site; PDB, Protein Data Bank; PEG200, poly(ethylene glycol) 200; (*RS*)-(±)-**3**, (*RS*)-(±)-*N*-9'-(1',2',3',4'-tetrahydroacridinyl)-*N'*-5"-[5'',6'',7'',8''-tetrahydro-2'(1'*H*)-quinolinonyl]-1,10-diaminododecane or (*RS*)-(±)-tacrine-(10)-hupryridone bis(oxalic acid); rmsd, root-mean-square deviation; SA, simulated annealing; STD, standard deviation; *Tc*, *Torpedo californica*; tacrine or **1**, 9-amino-1,2,3,4-tetrahydroacridine; FDA, U.S. Food and Drug Administration.
(2) Taylor, P. In *The Pharmacological Basis of Therapeutics*, 9th ed.; Hardman, J. G., Limbird, L. E., Molinoff, P. B., Ruddon, R. W., Gilman, A. G., Eds.; McGraw-Hill: New York, 1996; Vol., pp 161–176.

(3) Axelsen, P. H.; Harel, M.; Silman, I.; Sussman, J. L. *Protein Sci.* **1994**, *3*, 188–197.
(4) Ma, J. C.; Dougherty, D. A. *Chem. Rev.* **1997**, *97*, 1303–1324.
(5) Harel, M.; Schalk, I.; Ehret-Sabatier, L.; Bouet, F.; Goeldner, M.; Hirth, C.; Axelsen, P.; Silman, I.; Sussman, J. L. *Proc. Natl. Acad. Sci. U.S.A.* **1993**, *90*, 9031–9035.

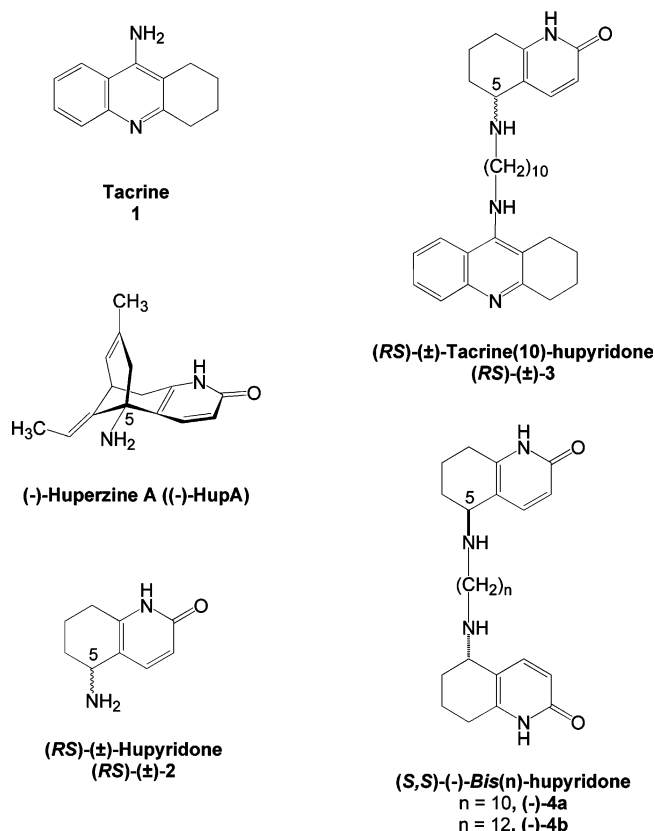


Figure 1. Chemical structures of the principal AChE inhibitors referred to in this study. C-5 in (RS)-(+)-**3** is chiral. Units that bind at the CAS or PAS are denoted with the subscript “cat” or “per”, respectively.

cholinergic hypothesis, ACh deficiency is associated with Alzheimer’s disease (AD). It was thus predicted that AChE inhibitors should ameliorate the effects of the disease.⁷ Such inhibitors were indeed shown to improve the cognitive abilities of early-stage AD patients,^{7,8} and all the first generation of AD drugs are anticholinesterase agents, including the alkaloids (–)-galanthamine (GAL, Reminyl)⁹ and (–)-huperzine A [(–)-HupA]^{10,11} and the synthetic compounds tacrine (**1**, Cognex),^{12,13} rivastigmine (Exelon),¹⁴ and E2020 (donepezil, Aricept)^{15–17} (Figure 1). The crystal structures of complexes of all these inhibitors with TcAChE and their modes of interaction with the enzyme have been determined.¹⁸

The “bivalent ligand” strategy involves the synthesis of drugs in which identical or different pharmacophores are linked via a suitable linker. This strategy takes advantage of the “chelate effect”¹⁹ to create a bifunctional ligand with enhanced affinity

for its target. The geometry of the active-site gorge, with specific sites at its two extremities, makes AChE a particularly attractive target for applying this approach. Even before the 3D structure of AChE was known, bivalent ligands such as decamethonium,²⁰ BW284C51,²¹ and ambenonium²² were described, which displayed both high affinity and high selectivity for this enzyme. Recent examples of successful utilization of this strategy include bis-(7)-tacrine²³ and the triazole-linked **1**/phenylphenanthridium-based inhibitor *syn*-TZ2PA6, which exhibits a 77 fM affinity for TcAChE.²⁴ The development of bivalent AChE inhibitors, as potential therapeutic drugs for AD, has been recently reviewed by Du and Carlier.²⁵ An important observation made in applying this strategy to AChE was that even pharmacophores with a weak affinity for AChE could still serve as effective peripheral-site ligands when incorporated into a bivalent drug.^{26,27} The design of one such pharmacophore, 5-amino-5,6,7,8-tetrahydroquinolinone (**2**, hupridone), is based on the naturally occurring, CAS inhibitor (–)-HupA (Figure 1).²⁸ Biochemical studies have shown that while monomeric **2** has no significant inhibitory effect on AChE activity, alkylene-linked dimers of **2** have twice the inhibition potency of the natural product.²⁸ X-ray crystal structures of TcAChE complexed with 10- and 12-carbon-tether-linked **2** dimers (*S,S*)-(–)-**4a** and (*S,S*)-(–)-**4b** (Figure 1) show one monomer bound at the CAS, the linker spanning the gorge, and the other monomer bound at the PAS.²⁹ In the spirit of the bivalent ligand strategy and in light of these findings, the inhibitor (RS)-(+)-*N*-9’-(1’,2’,3’,4’-tetrahydroacridinyl)-*N*-5’’-[5’’,6’’,7’’,8’’-tetrahydro-2’(1’*H*)-quinolinonyl]-1,10-diaminododecane [(RS)-(+)-**3**, (RS)-(+)-tacrine-(10)-hupridone] was designed and synthesized as a bisoxalate salt (Figure 1).³⁰ This heterodimer is composed of a 10-carbon linker connecting two pharmacophores, viz., **1** and **2** moieties. In the **2** unit, the carbon at position 5, which is connected to the 10-carbon linker, is a chiral center (Figure 1). The bis(oxalic acid) salt of this molecule was synthesized as the racemate, and thus included both the (*R*)- and the (*S*)-configured **2** units. (RS)-(+)-**3** displayed substantially higher affinity for rat AChE than monomeric **1**, (–)-HupA, or the dimers (*S,S*)-(–)-**4a** and (*S,S*)-(–)-**4b**, the IC₅₀ values being 8.8, 223, 114, 151, and 52 nM, respectively.^{28,30}

The 3D structures of the appropriate bivalent ligand/AChE complexes, determined by X-ray crystallography, have provided valuable structural insights.^{17,29} For example, the crystal structure of the E2020/TcAChE complex revealed that only the higher affinity enantiomer (*R*)-E2020 is bound.¹⁷ Bivalent inhibitors

- (6) Taylor, P.; Radic, Z. *Annu. Rev. Pharmacol. Toxicol.* **1994**, *34*, 281–320.
 (7) Bartus, R. T.; Dean, R. L.; Beer, B.; Lippa, A. S. *Science* **1982**, *217*, 408–414.
 (8) Giacobini, E. In *Cholinesterases and cholinesterase inhibitors*; Giacobini, E., Ed.; Martin Dunitz Ltd.: London, 2000; pp 181–226.
 (9) Greenblatt, H. M.; Kryger, G.; Lewis, T.; Silman, I.; Sussman, J. L. *FEBS Lett.* **1999**, *463*, 321–326.
 (10) Raves, M. L.; Harel, M.; Pang, Y.-P.; Silman, I.; Kozikowski, A. P.; Sussman, J. L. *Nat. Struct. Biol.* **1997**, *4*, 57–63.
 (11) Tang, X. C.; He, X. C.; Bai, D. L. *Drugs Future* **1999**, *24*, 647–663.
 (12) Watkins, P. B.; Zimmerman, H. J.; Knapp, M. J.; Gracon, S. I.; Lewis, K. W. *J. Am. Med. Assoc.* **1994**, *271*, 992–998.
 (13) Davis, K. L.; Powchik, P. *Lancet* **1995**, *345*, 625–630.
 (14) Bar-On, P.; Millard, C. B.; Harel, M.; Dvir, H.; Enz, A.; Sussman, J. L.; Silman, I. *Biochemistry* **2002**, *41*, 3555–3564.
 (15) Nightingale, S. L. *J. Am. Med. Assoc.* **1997**, *277*, 10.
 (16) Kawakami, Y.; Inoue, A.; Kawai, T.; Wakita, M.; Sugimoto, H.; Hopfinger, A. *J. Bioorg. Med. Chem. Lett.* **1996**, *4*, 1429–1446.
 (17) Kryger, G.; Silman, I.; Sussman, J. L. *Structure* **1999**, *7*, 297–307.
 (18) See the Supporting Information.

- (19) Jencks, W. P. *Adv. Enzymol. Relat. Areas Mol. Biol.* **1975**, *43*, 219–410.
 (20) Bergmann, F.; Wilson, I. B.; Nachmansohn, D. *Biochim. Biophys. Acta* **1950**, *6*, 217–224.
 (21) Austin, L.; Berry, W. K. *Biochem. J.* **1953**, *54*, 695–700.
 (22) Hodge, A. S.; Humphrey, D. R.; Rosenberry, T. L. *Mol. Pharmacol.* **1992**, *41*, 937–942.
 (23) Pang, Y.-P.; Quiram, P.; Jelacic, T.; Hong, F.; Brimijoin, S. *J. Biol. Chem.* **1996**, *271*, 23646–23649.
 (24) Lewis, W. G.; Green, L. G.; Grynszpan, F.; Radic, Z.; Carlier, P. R.; Taylor, P.; Finn, M. G.; Sharpless, K. B. *Angew. Chem., Int. Ed.* **2002**, *41*, 1053–1057.
 (25) Du, D. M.; Carlier, P. R. *Curr. Pharm. Des.* **2004**, *10*, 3141–3156.
 (26) Carlier, P. R.; Chow, E. S.-H.; Han, Y.-F.; Liu, J.; El Yazal, J.; Pang, Y.-P. *J. Med. Chem.* **1999**, *42*, 4225–4231.
 (27) Han, Y.-F.; Li, C. P.-L.; Chow, E.; Wang, H.; Pang, Y.-P.; Carlier, P. R. *Bioorg. Med. Chem. Lett.* **1999**, *7*, 2569–2575.
 (28) Carlier, P. R.; Du, D.-M.; Han, Y.-F.; Liu, J.; Perola, E.; Williams, I. D.; Pang, Y.-P. *Angew. Chem., Int. Ed.* **2000**, *39*, 1775–1777.
 (29) Wong, D. M.; Greenblatt, H. M.; Dvir, H.; Carlier, P. R.; Han, Y.-F.; Pang, Y.-P.; Silman, I.; Sussman, J. L. *J. Am. Chem. Soc.* **2003**, *125*, 363–373.
 (30) Carlier, P. R.; Du, D.-M.; Han, Y.-F.; Liu, J.; Pang, Y.-P. *Bioorg. Med. Chem. Lett.* **1999**, *9*, 2335–2338.

Table 1. X-ray Data Collection and Processing Statistics for Trigonal and Orthorhombic Crystals of the 3/TcAChE Complex

	trigonal form	orthorhombic form
space group	$P3_121$	$P2_12_12_1$
cell axes (Å, deg)	$a = b = 111.45, c = 137.10,$ $\alpha = \beta = 90, \gamma = 120$	$a = 91.00, b = 105.54, c = 150.45,$ $\alpha = \beta = \gamma = 90$
temp (K)	120	120
oscillation angle (deg)	0.5	0.5
total no. of frames	162	219
resolution range (Å)	30.0–2.30	40.0–2.10
no. of measured reflns	496 411	1 268 585
no. of unique reflns	44 250	84 805
no. of unique reflns used	43 557	84 288
completeness (%): all data (highest shell)	98.5 (99.7) ^a	99.4 (98.5) ^b
R_{merge} (%): all data (highest shell)	6.8 (36.7) ^a	7.8 (39.6) ^b
mean I/σ : all data	16.3	18.2
reflins in highest resolution shell with I/σ less than 3σ (%)	45.3	56.5

^a Highest resolution shell was 2.38–2.30 Å. ^b Highest resolution shell was 2.16–2.10 Å.

of AChE have now been proposed to be a disease-modifying agent rather than a mere palliative, because of the potential involvement of the PAS of AChE in increasing the deposition of β -amyloid ($A\beta$) into insoluble plaques.³¹ X-ray structures of bivalent-ligand/AChE complexes offer valuable information on molecular recognition at the PAS of AChE, and insight into the design of a new generation of AChE inhibitors as potential disease-modifying agents. In this study we present detailed structural information of AChE in complex with (*RS*)-(±)-**3**, and an unprecedented observation of enantiomeric selection of (*R*)-**3** mediated by crystal packing.³²

Experimental Section

Inhibitors and Other Chemicals. (*RS*)-**3** was prepared as described previously.³⁰ 2-[*N*-Morpholino]ethanesulfonic acid (MES) and poly(ethylene glycol) 200 (PEG200) were purchased from Sigma Chemicals (St. Louis, MO).

Crystallographic Data Collection. Native TcAChE trigonal crystals, prepared as described previously,^{29,33} were soaked in mother liquor (40% v/v PEG200 in 0.1 M MES, pH 5.8, 6 μ L drop) containing 2 mM (*RS*)-**3** at 4 °C for 17 h. TcAChE orthorhombic crystals³⁴ were soaked in mother liquor (40% v/v PEG200 in 0.1 M MES, pH 5.8, 6 μ L drop) containing 4 mM (*RS*)-**3** at 4 °C for 40 h. Crystals of both types were then transferred to Paratone-N oil (gift of H. Hope)³⁵ for cryoprotection, placed on a goniostat, and flash cooled to 120 K (Oxford Cryo-systems). The “in-house” X-ray source was a Rigaku RU-H3R rotating anode running at 50 kV/90 mA ($\lambda = 1.5418$ Å, Cu K α). Images were collected using a Rigaku R-Axis IV++ image plate detector.

Data collection was optimized by the program STRATEGY,³⁶ and the data were processed using DENZO and SCALEPACK.³⁷ Data were truncated with the CCP4 program TRUNCATE,³⁸ and a list of 5% randomly generated test reflections was taken from a master list using CAD and FREEFLAG.³⁸ Reflections for the trigonal crystal form were output with MTZ2VARIOUS³⁸ to a format suitable for the CNS_SOLVE package (version 1.1).³⁹ The orthorhombic crystal form

was refined and analyzed using CCP4.³⁸ Table 1 summarizes pertinent information concerning X-ray data collection and processing for both crystal forms.

Structure Determination and Refinement. Molecular models of (*RS*)-**3** were built using CS Chem3D Pro (version 7.0).⁴⁰ Energy minimization was performed on inhibitor models using the molecular dynamic utilities of CS Chem3D Pro.⁴⁰ These models were used to generate suitable topology and parameter files for CNS using AUTODIC from the XPLO2D program (version 001221/2.8.9)⁴¹ prior to map fitting.

The structure of the trigonal form of the (*RS*)-**3**/TcAChE complex was determined using the difference Fourier technique, exploiting the previously determined crystal structure of TcAChE (PDB ID 2ACE).^{10,18} All stages of refinement utilized CNS.³⁹ Rigid body refinement was performed, and subsequent maps were calculated, using data in the 30.0–2.3 Å resolution range. The initial *R* factor of 28.9% and R_{free} of 30.8% were reduced to 26.3% and 29.1%, respectively. Simulated annealing (SA; torsion dynamics mode)⁴² at 2500 K, with harmonic constraints for individual atoms, was then performed, followed by individual *B* factor refinement. At this stage, the *R* factor and R_{free} dropped to 20.9% and 24.5%, respectively. Stringent criteria were used for the assignment of water molecules; thus, long strings of electron density, which may correspond to parts of the PEG200 molecules, were not fitted, nor were peaks with no obvious H-bond donors/acceptors within 4 Å. The inhibitor and several carbohydrate molecules were gradually fitted. The map phases improved with subsequent cycles of model building, positional maximum-likelihood minimization, and *B* factor refinement, until the *R* factors converged (see Table 2 for summarized results).

The orthorhombic structure was solved by employing an unpublished orthorhombic structure as the starting model. Rigid body refinement was used to adjust each molecule in the asymmetric unit (AU) independently, followed by individual atom refinement. The noncrystallographic symmetry inherent in the asymmetric unit was not used in refinement. The program REFMAC5⁴⁴ from the CCP4 suite was used for refinement,³⁸ using data in the 40.0–2.10 Å resolution range. The *R* factor after initial refinement was 32.0%, and R_{free} was 33.9%. Molecular models of (*RS*)-**3** and the corresponding inhibitor library file, containing topological and parametric data, were generated using the monomer library sketcher module from the CCP4 suite,³⁸ prior to

- (31) Dorronsoro, I.; Castro, A.; Martinez, A. *Expert Opin. Ther. Pat.* **2003**, *13*, 1725–1732.
 (32) Henceforth, compounds (*RS*)-(±)-**3**, (*S,S*)-(-)-**4a**, and (*S,S*)-(-)-**4b** will be referred to as (*RS*)-**3**, (-)-**4a**, and (-)-**4b**, respectively.
 (33) Sussman, J. L.; Harel, M.; Frolow, F.; Oefner, C.; Goldman, A.; Toker, L.; Silman, I. *Science* **1991**, *253*, 872–879.
 (34) Greenblatt, H. M.; Guillou, C.; Guénard, D.; Argaman, A.; Botti, S.; Badet, B.; Thal, C.; Silman, I.; Sussman, J. L. *J. Am. Chem. Soc.* **2004**, *126*, 15405–15411.
 (35) Hope, H. *Acta Crystallogr.* **1988**, *B44*, 22–26.
 (36) Ravelli, R. B. G.; Sweet, R. M.; Skinner, J. M.; Duisenberg, A. J. M.; Kroon, J. *J. Appl. Crystallogr.* **1997**, *30*, 551–554.
 (37) Otwinowski, Z.; Minor, W. *Methods Enzymol.* **1997**, *276*, 307–326.
 (38) Bailey, S. *Acta Crystallogr.* **1994**, *D50*, 760–763.
 (39) Brünger, A. T.; Adams, P. D.; Clore, G. M.; DeLano, W. L.; Gros, P.; Grosse-Kunstleve, R. W.; Jiang, J. S.; Kuszewski, J.; Nilges, M.; Pannu, N. S.; et al. *Acta Crystallogr.* **1998**, *D54*, 905–921.

- (40) CS Chem3D Pro 7.0.0 and CS ChemDraw Ultra 7.0.1, CambridgeSoft Corp., 100 Cambridge Park Dr., Cambridge, MA 02140-2317, <http://www.camsoft.com>, 2001.
 (41) Kleywegt, G. J.; Jones, T. A. *Methods Enzymol.* **1997**, *277*, 208–230; <http://xray.bmc.uu.se/gerard/gmrp/gmrp.html>.
 (42) Brünger, A. T.; Adams, P. D.; Rice, L. M. *Prog. Biophys. Mol. Biol.* **1999**, *72*, 135–155.
 (43) Laskowski, R. A.; MacArthur, M. W.; Moss, D.; Thornton, J. M. *J. Appl. Crystallogr.* **1993**, *26*, 283–291.
 (44) Murshudov, G. N.; Vagin, A. A.; Dodson, E. J. *Acta Crystallogr.* **1997**, *D53*, 240–255.

Table 2. Refinement and Model Statistics for 3/TcAChE Structures

	trigonal form	orthorhombic form ^b
resolution range (Å)	29.2–2.30	40.0–2.10
no. of reflns	43 555	80 089
R_{work}^a (%)	18.8	19.6
R_{free} (5% of reflns) ^a (%)	22.9	24.7
no. of protein atoms	4176	4174 (A) + 4195 (B) ^b
no. of nonprotein atoms		
solvent (water)	178	173 (A) + 168 (B) ^b
carbohydrate	28	42 (A) + 28 (B) ^b
inhibitor	37	37 (A) + 37 (B) ^b
B factor (Å ²): av/ σ /min/max		
protein	38.1/8.1/20.7/73.8	26.16/7.49/9.57/63.98 (A) ^{b,c} 25.50/7.76/9.27/65.43 (B) ^{b,c}
water molecules	39.6/7.3/14.7/63.0	25.05/5.99/12.55/46.66 (A + B) ^{b,c}
carbohydrate	63.7/8.1/52.9/76.0	56.90/13.05/37.42/78.22 (A + B) ^{b,c}
inhibitor	46.3/5.7/38.1/53.7	28.04/6.85/16.81/41.25 (A) ^{b,c} 29.19/6.29/19.92/41.90 (B) ^{b,c}
RMS bond length dev (Å)	0.019	0.036
RMS bond angle dev (deg)	1.92	2.506
agreement with Ramachandran plot ^d	89.1% in the most favorable region; two residues in the generously allowed region	89.9% in the most favorable region; three residues in the generously allowed region
PDB accession code	1ZGB	1ZGC

^a All the output reflections from TRUNCATE were used in the refinement, with no σ cutoff. ^b In the orthorhombic form, chains A and B refer to the two noncrystallographic 2-fold axis-related dimer molecules in the AU and their associated/corresponding nonprotein atoms and molecules. ^c Inhibitor molecules bound to protein molecule chains A and B in the orthorhombic structure. ^d Analysis done with PROCHECK.⁴³

map fitting.³⁸ Water molecules, the bound inhibitor, and several carbohydrate molecules were assigned and gradually fitted into the electron density maps as described above for the trigonal form.

Simulated annealing omit maps (SA at 1000 K, torsion dynamics mode), for both the trigonal and orthorhombic crystal forms, were produced for the refined structures with CNS³⁹ with the ligand atoms omitted from the map calculations. Unless otherwise stated, all atoms for the structures were refined with an occupancy of 1.0. Final refinement parameters for both crystal forms are presented in Table 2. The program XtalView (version 4.0) and its utilities⁴⁵ were used for all model building, and X-ray crystal structures of TcAChE and of its complexes were compared using LSQMAN (version 010126/7.7.1).⁴⁶ The coordinates of both refined structures and the corresponding structure factors have been submitted to the PDB (ID codes 1ZGB and 1ZGBSF for the trigonal form; 1ZGC and 1ZGCSF for the orthorhombic form). Unless otherwise stated, images of the X-ray structures were generated with Xfit⁴⁵ and Raster3D,⁴⁷ and chemical structures were created with CS ChemDraw Ultra (version 7.0.1).⁴⁰

Results

Trigonal Crystal Form. The calculated initial difference map ($F_o - F_c$) for the trigonal crystal form displayed well-defined electron density for the 1 unit (1_{cat}) of (RS)-3 near the bottom of the gorge, adjacent to the CAS. Electron density due to the alkylene linker was mostly visible, and can be seen to span the length of the gorge. Initially, only the 1_{cat} ring system was fitted, to avoid model bias. Some side chains outside the active-site gorge were also removed for the same reason. The side chain of residue Phe330, which appeared within negative electron density, was moved and fitted into the proximal positive density. It was found that the (R)-2 unit (R)-2_{per}, with pseudoequatorial conformation at C-5, best fitted the ligand electron density near the top of the gorge at the PAS. The (S)-2_{per} unit could not be successfully modeled into the visible electron density, and thus cannot form similar H-bonds as seen for the (R)-2_{per} unit. The

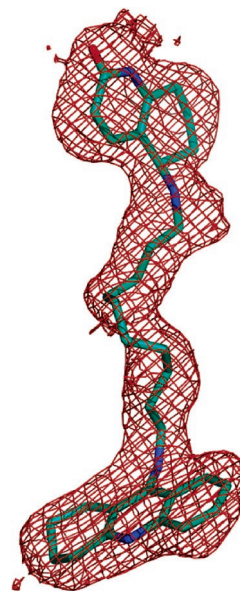


Figure 2. View of the refined structure of (R)-3 (cyan) in the active-site gorge of TcAChE (trigonal crystal form). The simulated annealing omit $2F_o - F_c$ map contoured at 3σ is shown as red mesh.

10-carbon linker was gradually built into the ligand electron density, as the map phases improved upon further model building and several cycles of refinement. Two *N*-acetyl-D-glucosamine (NAG) molecules and water molecules were also fitted. The SA omit map ($2F_o - F_c$) generated for the final refined structure shows full electron density for the complete inhibitor (Figure 2).

The protein backbone in the (R)-3/TcAChE complex is very similar to that in crystals of native trigonal TcAChE (PDB IDs 2ACE and 1EA5), and to crystal structures of complexes of TcAChE with other inhibitors, such as (–)-4a, (–)-4b, and 1 (PDB codes 1H22, 1H23, and 1ACJ, respectively).¹⁸ The average root-mean-square deviation (rmsd) for the α carbon (C_α) atoms was calculated for a set of TcAChE crystal structures.

(45) McRee, D. E. *J. Struct. Biol.* **1999**, *125*, 156–165.

(46) Kleywegt, G. J.; Jones, T. A. *ESF/CCP4 Newsl.* **1994**, *31* (Nov 9–14); http://xray.bmc.uu.se/usf/factory_4.html.

(47) Merritt, E. A.; Bacon, D. J. *Methods Enzymol.* **1997**, *277*, 505–524.

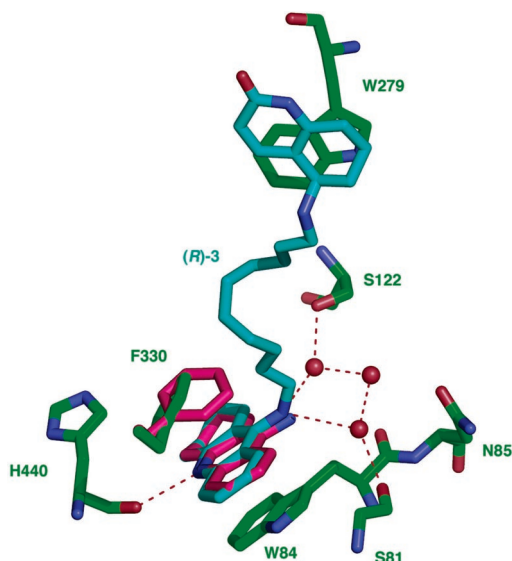


Figure 3. Overlay of the **1** (magenta) and (*R*)-**3** (cyan) complexes, showing the mode of binding of the **1** moiety at the CAS. Steric clash with the 10-carbon linker might explain the tilt observed for the Phe330 side chain (purple in the **1**/TcAChE structure). Residues for the trigonal (*R*)-**3**/TcAChE structure are rendered in green; water molecules are shown as red spheres. The image was created with PyMol.⁴⁸

These included, in addition to the trigonal (*R*)-**3**/TcAChE structure, native trigonal TcAChE, and the corresponding inhibitor complexes with (–)-**4a**, (–)-**4b**, and **1**, native orthorhombic crystals and corresponding complexes with a GAL derivative³⁴ and with (*RS*)-**3** (PDB codes 1W75, 1W76, and 1ZGC, respectively). The average rmsd value thus obtained was 0.28 ± 0.08 Å (for ~527 residues). See the Supporting Information¹⁸ for the similar TcAChE structures and for the data resulting from the structural comparisons.

A comparison of the trigonal (*R*)-**3**/TcAChE structure with the previously reported crystal structure of **1**/TcAChE^{5,18} shows a similar mode of binding for the **1**_{cat} moiety (Figure 3). In both structures the **1** ring system is located at the CAS, sandwiched between the aromatic side chains of Trp84 and Phe330 (π – π stacking). The phenyl ring of Phe330 is tilted in the (*R*)-**3**/TcAChE structure, relative to the **1**/TcAChE structure, probably due to steric hindrance imposed by the **3** linker. The **1**_{cat} unit of (*R*)-**3** makes a H-bond interaction of its protonated nitrogen with His440 O (3.0 Å) similar to that of **1** itself. Moreover, a system of three water molecules at the CAS binds the tacrine-linker nitrogen via H-bonds to Ser81 O, Asp72 O^{δ2}, Ser122 O^γ, and Asn85 O^{δ1} (2.6–3.5 Å), just as is seen in the **1**/TcAChE structure.⁵

The 10-carbon linker winds its way up the gorge with mixed anti and gauche conformers. At the PAS, the protonated nitrogen linking the (*R*)-**2** moiety and the 10-carbon linker does not form any apparent H-bonds. However, it can impart its positive charge on the neighboring carbons, to create an entity that makes a cation– π interaction with the indole ring of Trp279 (Figure 3). The distances between the centroid of the indole ring and the linker α -CH₂ carbon, nitrogen, and chiral C-5 carbon atoms of (*R*)-**2**_{per} are 4.8, 4.7, and 3.7 Å, respectively. A similar type of interaction is also observed at the CAS between the indole ring of Trp84 and the (*S*)-**2**_{cat} unit, in the previously reported structures of the complexes of (–)-**4a** and (–)-**4b** with TcAChE.^{18,29} Interestingly, the (*R*)-**2**_{per} moiety of (*R*)-**3** does not

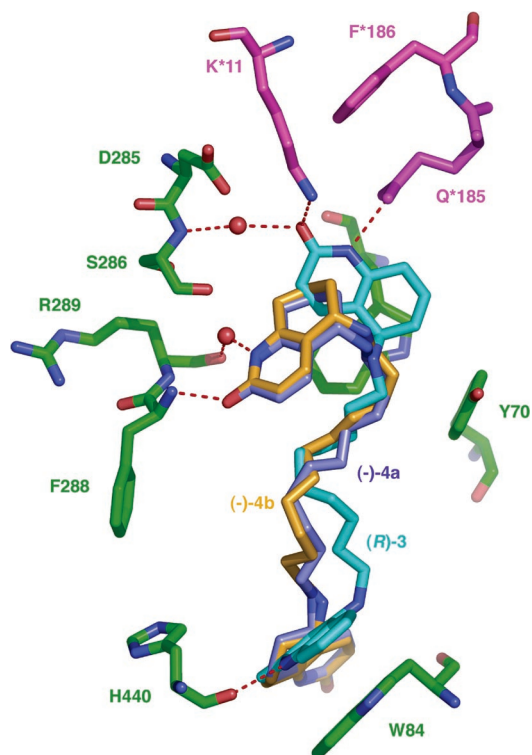


Figure 4. Superposition of the (*R*)-**3** (cyan) and (*S,S*)-(-)-**4b** (gold) and (*S,S*)-(-)-**4a** (purple) complexes showing the mode of binding of the **2** moiety. Trigonal TcAChE residues are rendered in green, symmetry-related TcAChE residues are rendered in magenta, and water molecules are shown as red spheres. The image was created with PyMol.⁴⁸

curl back upon itself as was observed for the (*S*)-**2**_{per} moiety in the (–)-**4a**/TcAChE and (–)-**4b**/TcAChE structures (Figure 4).²⁹ The optimal *R* factor for the (*R*)-**3**/TcAChE structure was achieved with a ligand occupancy of 0.9.

An interesting feature of the (*R*)-**3**/TcAChE complex, which might offer an explanation for the observed enantiomeric selectivity, is the occurrence of two direct H-bonds connecting the pyridone O of (*R*)-**2**_{per} to Lys11 N^ε and its pyridone N to Gln185 O^{ε1} of a symmetry-related molecule, with lengths of 2.9 and 2.8 Å, respectively. Another H-bond connects the (*R*)-**2**_{per} pyridone O to a water molecule (2.8 Å), which is bound to Ser286 N (3.0 Å) near the mouth of the gorge. As previously reported,²⁹ the (*S*)-**2**_{per} unit of both (–)-**4a** and (–)-**4b** forms both a direct and an indirect H-bond with the protein backbone in the PAS region (Figure 4): one between the pyridone O and Phe288 N, and the other between the pyridone N and a water molecule that is bound to Arg289 O (2.7–2.9 Å). Assuming similar interactions for the (*S*)-**2**_{per} unit in (*S*)-**3**, the three H-bonds observed for the (*R*)-**2**_{per} unit in (*R*)-**3**/TcAChE should make the complex thermodynamically more stable than the two that are assumed to be made by the (*S*)-**2**_{per} unit. This may explain why the (*R*)-enantiomer predominates in the case of the **3**/TcAChE complex.

Orthorhombic Crystal Form. To examine whether the symmetry-related interaction described above is the cause of the apparent enantiomeric selectivity, we soaked a different crystal form of TcAChE with the **3** racemate. An orthorhombic crystal form was chosen in which the surface of the protein at the mouth of the gorge (the PAS Trp279–Phe290 loop region) does not interact as closely with a symmetry-related TcAChE molecule in the AU as in the trigonal form.^{18,34} The structure

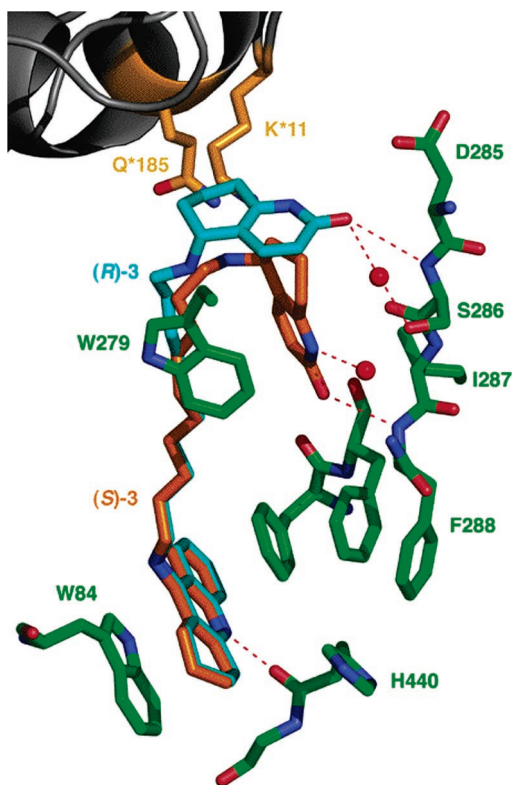


Figure 5. (*R*)-**3** (cyan) and (*S*)-**3** (orange) bound within the active-site gorge of *TcAChE* in the orthorhombic crystals. Selected enzyme residues and side chains are highlighted in green; water molecules are shown as red spheres. The symmetry-related side chains of Gln*185 and Lys*11 (yellow) shown at the top do not hydrogen bond to the inhibitor. The image was created with PyMol.⁴⁸

of the (*RS*)-**3**/*TcAChE* complex in this orthorhombic crystal revealed an overall protein backbone very similar to that in both the native trigonal and native orthorhombic *TcAChE* crystals (see above). The two copies of the protein in the AU of the orthorhombic crystal are very similar to each other, with a C_{α} rmsd value of 0.17 Å for 527 residues.¹⁸ The structure reveals a 1_{cat} moiety bound at the CAS in an orientation similar to that reported previously for **1**,^{5,18} which makes protein–ligand and water–ligand interactions similar to those in the trigonal form described above. However, relative to its conformation in the trigonal form, the 10-carbon linker of **3** in the orthorhombic structure traces a more direct trajectory up the gorge (cf. Figure 5 vs Figure 3).

The inhibitor molecules in the two copies of the protein in the AU have essentially identical orientations and conformations. During the initial stages of refinement, no electron density was visible in the PAS region that might correspond to either 2_{per} enantiomer. In subsequent cycles of refinement, some electron density appeared in proximity to Arg289 and Ser286 in both copies of the AU. This electron density was sufficient to model in the (*S*)- 2_{per} moiety of the (*S*)-**3** enantiomer, with a pseudo-equatorial conformation at C-5, its positioning being similar to that of the (*S*)- 2_{per} unit in both the (–)-**4a**/*TcAChE* and (–)-**4b**/*TcAChE* complexes.^{18,29} However, it was impossible to fit the (*R*)- 2_{per} entity into this electron density. As was predicted, the (*S*)- 2_{per} unit of **3** at the PAS is seen to bend back into the gorge, forming a H-bond through its pyridone O to Phe288 N (~ 3.2 Å; cf. 2.7 Å for (–)-**4a,b**). The pyridone N of (*S*)- 2_{per} makes a H-bond to a water molecule (~ 2.7 Å; cf. 2.7–2.9 Å

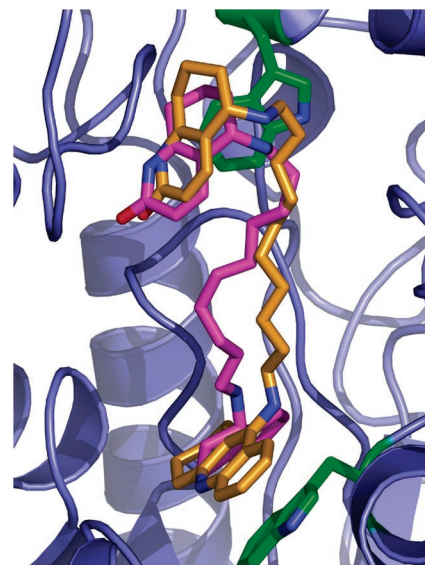


Figure 6. An overlay of (*S,S*)-(-)-**4a** (magenta) and (*S*)-**3** (orange, orthorhombic *TcAChE*) showing the similar binding mode of the (*S*)- 2_{per} unit at the PAS. The side chains of Trp279 (top) and Trp84 (bottom) are rendered as green sticks, at the PAS and the CAS, respectively. The protein backbone is displayed as a ribbon diagram (indigo). The image was created with PyMol.⁴⁸

for (–)-**4a,b**) that is H-bonded to Arg289 O (~ 2.9 Å; cf. 2.7–2.8 Å for (–)-**4a,b**) (Figure 5). The protonated 5-amino N and linker α -CH₂ carbon, as an entity, make a cation– π interaction with the pyrrole ring of Trp279 (distances between the pyrrole centroid and the nitrogen and α -CH₂ carbon atoms of (*S*)- 2_{per} are ~ 5.9 and ~ 4.5 Å, respectively; cf. ~ 5.3 and ~ 3.9 Å, respectively, for (–)-**4a,b**). Comparison of the H-bond and cation– π distances for the protein–ligand contacts of the (*S*)- 2_{per} unit of (*S*)-**3**, and the corresponding contacts in the (–)-**4a** and (–)-**4b** structures, indicates that the (*S*)-**3** enantiomer makes relatively weaker contacts at the PAS.²⁹ Figure 6 shows an overlap of the (*S*)- 2_{per} moiety in the (*S*)-**3**/*TcAChE* and (–)-**4a**/*TcAChE* complexes.

In later stages of refinement, more electron density appeared in the difference $F_o - F_c$ map above the fitted (*S*)- 2_{per} unit of **3**. The (*R*)- 2_{per} unit (with pseudo-equatorial conformation at C-5), but not the (*S*)- 2_{per} unit, could be fitted into this electron density (Figure 7). In both molecules of the AU, the pyridine O of this (*R*)- 2_{per} unit can form a H-bond with Ser286 N (2.8 ± 0.1 Å); only in one of them, however, does it form a H-bond (2.3 Å) with a water molecule that is H-bonded (2.7 Å) to Ser286 O' (Figure 5). Notably, it does not form H-bonds with any residues of the symmetry-related enzyme molecule. Its protonated 5-amino N and linker α -CH₂ carbon, as an entity, appear to form stronger cation– π interactions with the pyrrole ring of Trp279 (distances between the pyrrole centroid and the nitrogen and α -CH₂ carbon atoms of (*R*)- 2_{per} are ~ 3.9 and ~ 4.4 Å, respectively), both substantially shorter than the corresponding bonds made by the (*S*)- 2_{per} moiety (see above). It should also be noted that there was insufficient electron density to fit the (*R*)- 2_{per} unit into the $F_o - F_c$ SA omit map calculated for the final orthorhombic structure, relative to the (*S*)- 2_{per} unit (see Figure S5 in ref 18). These observations can be accounted for by assuming that the two enantiomers bind inside the gorge with roughly equal affinity. Thus, the lower part of the inhibitor has good electron density. The (*S*)- 2_{per} unit is present at only

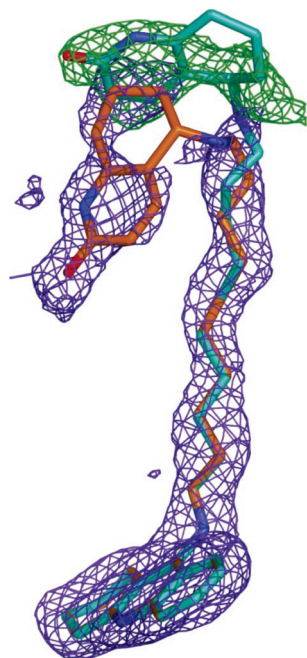


Figure 7. View of refined structures of (*S*)-**3** (gold stick) and (*R*)-**3** (cyan stick) fitted into the $2F_o - F_c$ (blue mesh) and $F_o - F_c$ (green mesh) maps of the orthorhombic TcAChE crystal form, both contoured at 2σ .

$\sim 50\%$ occupancy, and so has visible but weak density. The (*R*)-**2**_{per} unit, also present at $\sim 50\%$ occupancy, is not constrained in the gorge, and is quite mobile, or has a multipoint interaction at the mouth of the gorge, giving rise to very weak electron density (Figure 7). The final refined structure contains the (*S*)-**3** enantiomer with the (*S*)-**2**_{per} unit with 50% occupancy for both molecules in the AU.

Discussion

Enantiomeric selectivity by enzymes is a fundamental issue in drug development. The possibility of two enantiomers of the same drug having different pharmacological properties makes it necessary to thoroughly investigate each enantiomer in a newly developed chiral drug, as required by the U.S. Food and Drug Administration (FDA).⁴⁹ In the context of drug development, an inherent preference of an enzyme for one enantiomer would render inhibition by the racemate less effective than inhibition by the preferred enantiomer, as is the case for HupA.^{50,51} In the case of the anti-AD drug E2020, the (*R*)-enantiomer is reported to be slightly more potent ($K_i = 3.35$ nM) than the (*S*)-enantiomer ($K_i = 17.5$ nM, species not specified).⁵² On the basis of this published 5-fold ratio of enantiomer affinities, the selective complexation of the (*R*)-enantiomer by TcAChE observed in the X-ray crystal structure^{17,53} was unexpected. However, the preferential binding of the (*R*)-enantiomer from the solution of racemic E2020 could easily be rationalized if TcAChE were slightly more enantioselective (e.g., K_i ratio > 20)

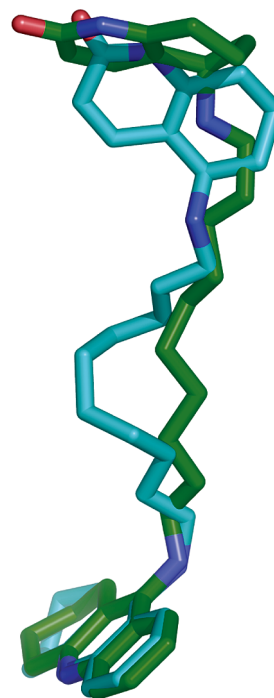


Figure 8. View of refined structures of (*R*)-**3** (cyan, (*R*)-**2**_{per} unit “parallel” form, trigonal) and (*R*)-**3** (green, (*R*)-**2**_{per} unit “perpendicular” form, orthorhombic) in the two crystal forms of TcAChE, showing the different binding orientations of the (*R*)-**2**_{per} unit at the PAS. The image was created with PyMol.⁴⁸

than the AChE species used in the published kinetic studies. Thus, the enantioselectivity demonstrated in our previous work appears to be due to an inherent binding preference of one enantiomer within the active-site gorge of the enzyme.

In contrast, the present work suggests a completely different origin of enzymic enantioselectivity. Our data show the trigonal crystals of TcAChE, soaked in a racemic mixture of **3**, selectively bind the (*R*)-enantiomer, whereas the orthorhombic crystals do not display this selectivity. Thus, the enzyme clearly does not have a substantial inherent preference for either of the two enantiomers of **3**. This dichotomy supports the hypothesis that the apparent selectivity of the trigonal crystals indeed stems from crystal packing and crystal contacts. Typically, in the energy range of 4–48 kJ/mol, hydrogen bonds serve as significant stabilizers of structure in terms of protein folding.⁵⁴ Although there is no apparent reason to preclude binding of the (*S*)-enantiomer in the trigonal form a priori, there appears to be a thermodynamic preference for the binding of the (*R*)-enantiomer, possibly due to the two H-bonds modeled for the (*S*)-**2**_{per} moiety vs three H-bonds observed for the (*R*)-**2**_{per} moiety. As such, the exclusive binding of the (*R*)-enantiomer is reasonable, given the long soaking time and the reversible nature of binding, which allow the system to reach a thermodynamic equilibrium. The orthorhombic structure provides further insight: the two H-bonds formed by both **2**_{per} enantiomers of **3** do not provide a strong thermodynamic advantage for either of them. Furthermore, the (*S*)-**2**_{per} unit forms two H-bonds through its two atoms while the (*R*)-**2**_{per} unit forms two H-bonds through one atom. This would likely allow greater mobility of the (*R*)-**2**_{per} moiety and may

(48) DeLano, W. L. *The PyMOL Molecular Graphics System*, 0.95; DeLano Scientific: San Carlos, CA, 2002; <http://pymol.sourceforge.net/>.

(49) U.S. Food and Drug Administration—Center for Drug Evaluation and Research. <http://www.fda.gov/cder/guidance/stereo.htm>, May 1, 1992.

(50) McKinney, M.; Miller, J. H.; Yamada, F.; Tuckmantel, W.; Kozikowski, A. P. *Eur. J. Pharmacol.* **1991**, *203*, 303–305.

(51) Saxena, A.; Qian, N.; Kovach, I. M.; Kozikowski, A. P.; Pang, Y.-P.; Vellom, D. C.; Radic, Z.; Quinn, D.; Taylor, P.; Doctor, B. P. *Protein Sci.* **1994**, *3*, 1770–1778.

(52) Inoue, A.; Kawai, T.; Wakita, M.; Imura, Y.; Sugimoto, H.; Kawakami, Y. *J. Med. Chem.* **1996**, *39*, 4460–4470.

(53) Kryger, G.; Silman, I.; Sussman, J. L. *J. Physiol. (Paris)* **1998**, *92*, 191–194.

(54) van Holde, K. E.; Johnson, W. C.; Ho, P. S. *Principals of Physical Biochemistry*; Prentice Hall Inc.: Upper Saddle River, NJ, 1998; pp 103–107.

explain why it is practically invisible in the orthorhombic omit map.

Features such as the dual binding to Trp84 and Trp279, and the modes of binding of **1** and of the (*S*)-**2**_{per} moiety, have been analyzed in detail previously.^{5,29} The new features revealed in the present structures are the two binding modes of the (*R*)-**2**_{per} moiety of **3**: (1) a “parallel” conformation, in which the (*R*)-**2**_{per} unit is aligned parallel to the gorge axis, reaching out to, and contacting, a proximal symmetry-related enzyme molecule in the trigonal crystal; (2) a “perpendicular” conformation, in which the (*R*)-**2**_{per} unit, perpendicularly aligned relative to the gorge axis, is H-bonded only to one enzyme molecule in the orthorhombic crystal (Figure 8). The former is probably an artifact of the crystal state, and is unlikely to exist in solution, unless, perhaps, in an oligomeric structure where the proximity of the gorge’s mouth to another subunit allows such an interaction. Our data lend further support to the multipoint interaction first suggested for the (*R*)-**2**_{per} unit of (*R,R*)-(+)-**4b**, which exhibits 60-fold less potency as an inhibitor than the (*S,S*)-(–)-**4b** enantiomer for rat AChE.^{25,28}

Finally, it is worth noting that several recent papers advocate the development and use of dual-purpose inhibitors for both the palliative treatment of AD and retarding the progression of the disease (see refs 25 and 55–58 and references therein). Inhibitors which selectively bind to the PAS, or to both the CAS and PAS simultaneously, have the capacity not only to ameliorate the cholinergic deficiency associated with AD, but also to inhibit the aggregation of A β peptides, and thus to retard amyloid plaque formation. Since the (*R*)- and (*S*)-**3** inhibitors exhibit different modes of binding to the PAS, it will be worth examining whether they may differentially contribute to acceleration or retardation of AChE-induced A β aggregation. Future work will thus include evaluation of the enantiomerically pure forms of **3** and homologues for such potential therapeutic properties.

Conclusions

In this study we were able to demonstrate by X-ray crystallographic methods that protein–ligand interaction with a

proximal symmetry-related *TcAChE* molecule covering the entrance to the active-site gorge in trigonal crystals was responsible for the enantioselection of (*R*)-**3** from a racemic solution. In orthorhombic *TcAChE* crystals, in which the symmetry-related *TcAChE* molecule is less proximal to its entrance, this preference is not seen.

Acknowledgment. This project was supported by Research Grant Council (HK) Competitive, Earmarked Research Grant HKUST6236/99M, the Alzheimer’s and Related Disease Award Fund (Commonwealth of Virginia, Grant 03-1), the U.S. Army Medical and Material Command under Contract No. DAMD17-97-2-7022, the EC 5th Framework Program on the Quality of Life and Management of Living Resources, the Kimmelman Center for Biomolecular Structure and Assembly (Rehovot, Israel), the Benozziyo Center for Neurosciences, and the Kalman and Ida Wolens Foundation. J.L.S. is the Pickman Professor of Structural Biology. The orthorhombic crystals of *TcAChE* were a generous gift of Dr. Simone A. Botti and Anat Argaman (BioStrx Ltd., Ramat-Gan, Israel). We thank Lilly Toker, Boris Brumshtein, and Orna Man (Weizmann Institute of Science) for their assistance, and Prof. Mingjie Zhang and Prof. Yifan Han (Department of Biochemistry, Hong Kong University of Science and Technology, Hong Kong) for their support. The TOC graphics image was created with DINO.⁵⁹

Supporting Information Available: (1) List of PDB accession codes and AChE structures discussed in this study, (2) complete citation for references used in the main paper with more than 10 authors, (3) structural comparisons made between *TcAChE* and various inhibitor complexes, (4) quantitative comparison of symmetry-related contacts in the trigonal and orthorhombic crystal forms of *TcAChE*, (5) morphing movie of point 4, created with PyMol,⁴⁸ and (6) additional illustrations of the interaction of AChE inhibitors in the active-site gorge of *TcAChE* and X-ray structures of **3**/*TcAChE*. This material is available free of charge via the Internet at <http://pubs.acs.org>.

JA051765F

- (55) Colombres, M.; Sagal, J. P.; Inestrosa, N. C. *Curr. Pharm. Des.* **2004**, *10*, 3121–3130.
(56) Munoz-Muriedas, J.; Lopez, J. M.; Orozco, M.; Luque, F. J. *Curr. Pharm. Des.* **2004**, *10*, 3133–3140.

- (57) Bolognesi, M. L.; Andrisano, V.; Bartolini, M.; Banzi, R.; Melchiorre, C. *J. Med. Chem.* **2005**, *48*, 24–27.
(58) Rosini, M.; Andrisano, V.; Bartolini, M.; Bolognesi, M. L.; Hrelia, P.; Minarini, A.; Tarozzi, A.; Melchiorre, C. *J. Med. Chem.* **2005**, *48*, 360–363.
(59) Philippsen, A. *DINO: Visualizing Structural Biology*; Biozentrum: University of Basel, Switzerland; 2003; <http://www.dino3d.org>.